

Study of the Inhibitor of the Crayfish Neuromuscular Junction by Presynaptic Voltage Control

ANDREY VYSHEDSKIY AND JEN-WEI LIN

Department of Biology, Boston University, Boston, Massachusetts 02215

Vyshedskiy, Andrey and Jen-Wei Lin. Study of the inhibitor of the crayfish neuromuscular junction by presynaptic voltage control. *J. Neurophysiol.* 77: 103–115, 1997. The inhibitor of the crayfish opener muscle was investigated by a presynaptic voltage control method. Two microelectrodes were inserted into the inhibitor and the amplitude and duration of presynaptic depolarization were controlled by a voltage-clamp amplifier. The inhibitory postsynaptic potential (IPSP) was measured from a muscle fiber located near the presynaptic voltage electrode. Nonlinear summation of IPSP amplitudes was corrected after chloride equilibrium potential was measured. With the use of 5-ms presynaptic pulses, the depolarization-release coupling (D-R) curve constructed from IPSP peak amplitudes ($IPSP_{cor}$) had a threshold of about -35 mV and reached its maximal level at -5 to -10 mV. Depolarization beyond the maximum led to a suppression of neurotransmitter release. When transmitter release during a presynaptic pulse was completely suppressed, IPSPs activated by tail current could be identified with an average synaptic delay of 2.5 ms. Transmitter secretion triggered by a calcium current activated during the 5-ms pulses ($IPSP_{on}$) was also measured on the rising phase of an IPSP, at 2.5 ms after the end of the 5-ms pulses. D-R coupling plots measured from $IPSP_{on}$ exhibited a more pronounced suppression than that obtained from $IPSP_{cor}$. The effect of presynaptic pulse duration on the level of transmitter release was analyzed. Transmitter release increased with increasing duration and was nearly saturated by 20-ms pulses depolarized to 0 mV. The following conditions were identified as necessary to obtain a consistent D-R curve with a clear suppression: 1) small animals, 3.8 cm head to tail, 2) 15°C , 3) 40 mM tetraethylammonium and 1 mM 4-aminopyridine, 4) an extracellular calcium concentration of ≤ 10 mM. In addition, a consistent correlation was found among the branching pattern of the inhibitor, the placement of the presynaptic electrode, and the characteristics of the D-R curves. An ideal presynaptic electrode configuration involved placing the voltage electrode in a secondary branch, ~ 100 μm from the main branch point, and placing the current electrode at the branch point. Postsynaptically, optimal recordings were obtained from muscle fibers innervated by a single branch of the inhibitor that originated from a point near the presynaptic voltage electrode. A cable-release model was constructed to evaluate the relationship between the shape of the D-R coupling curves and the space constants of the presynaptic terminals. A comparison between the model and the D-R coupling curves suggested that the space constant of an inhibitor branch on a muscle fiber is ≥ 8 times longer than its actual length. Therefore the upper limit estimate of the space constant of a typical preparation is ~ 3 mm. Results reported here outline morphological and physiological conditions needed to achieve optimal control of the presynaptic branch of the crayfish inhibitor. The cable-release model quantitatively defines the extent of presynaptic voltage control.

INTRODUCTION

Biophysical and molecular mechanisms of neurotransmitter secretion processes have been an active area of research in neuroscience for several decades (for recent reviews see

Schweizer et al. 1995; Sudhof 1995). Because of the small dimensions of presynaptic terminals, their electrophysiological manipulation has always been difficult to achieve. At present, the squid giant synapse is the most consistently used preparation for the quantitative study of presynaptic mechanisms (Augustine et al. 1985a,b; Katz and Miledi 1969; Llinás et al. 1981a,b; Takeuchi and Takeuchi 1962). Attempts to develop alternative preparations have met with varying degrees of success, but none of these preparations has become popular (Blight and Llinas 1981; Brosius et al. 1990; Dietzel et al. 1986; Hayashi et al. 1985; Haydon 1988; Lin and Llinas 1993; Wojtowicz and Atwood 1984). However, the squid giant synapse is a phasic synapse responsible for the escape reflex and it exhibits very little synaptic plasticity under physiological conditions (Charlton et al. 1982; Swandulla et al. 1991). In the light of these constraints, we have sought to refine one of the alternative preparations, namely the crayfish opener muscle, because it has the following advantages: first, extensive studies have been conducted in this preparation and a solid data base already exists (Atwood and Wojtowicz 1986); second, the synapses on the opener muscle are of the low release probability type that exhibits an entire spectrum of synaptic plasticity under physiological conditions (Atwood et al. 1989; Bittner 1989); and last, the crayfish preparation allows limited electrophysiological access to the presynaptic terminal (Sivaramakrishnan et al. 1991; Wojtowicz and Atwood 1984). Although the majority of studies at the crayfish opener neuromuscular junction center on the excitor, the database for the inhibitor is also extensive. For example, it has been shown that the inhibitor exhibits a strong facilitation (Atwood and Bittner 1970; Dudel and Kuffler 1961a). The inhibitor is also the first preparation in which presynaptic inhibition was demonstrated (Dudel and Kuffler 1961b; Fuchs and Getting 1980). Quantitative ultrastructural study of the inhibitor has been carried out (Govind et al. 1995). Biochemical and pharmacological characterizations of γ -aminobutyric acid (GABA) metabolism as well as GABA-mediated chloride currents have also been studied extensively (Adelsberger et al. 1996; Dudel and Hatt 1976; Finger and Stettmeier 1981; Golan and Grossman 1994; Kaila and Voipio 1987). The inhibitor is chosen for our presynaptic voltage control approach specifically to avoid the muscle contraction that occurs if one tries to depolarize the excitor with large and prolonged pulses.

Gaining access to the presynaptic element by two intracellular electrodes allows one to precisely control the amplitude of presynaptic depolarization and, therefore, the number of

calcium channel openings. Such control provides a unique advantage over action potentials because one can now manipulate presynaptic calcium influx either by changing the number of open channels or by changing extracellular Ca^{2+} concentration ($[\text{Ca}^{2+}]_o$). This flexibility has been used to investigate the calcium cooperativity of transmitter release at the squid giant synapse (Augustine et al. 1985a; Llinás et al. 1981b). However, because of the lack of robust synaptic plasticity at the squid giant synapse, the impact of varying the number of calcium channel openings, and therefore the spatial profile of calcium distribution at a microscopic level, on synaptic facilitation has only been explored on theoretical grounds (Simon and Llinás 1985; Yamada and Zucker 1992). The implementation of the voltage control method on the crayfish inhibitor provides a starting point from which to understand the importance of the spatial profile of calcium influx during facilitation. In addition, control over the duration of presynaptic depolarization has the advantage of allowing one to study the interaction between synaptic facilitation and the dynamics of synaptic vesicle secretion during a continuous presynaptic depolarization (Borges et al. 1995; Llinás et al. 1981b; Simon and Llinás 1985). The added flexibility in the control of presynaptic waveforms provides an opportunity to explore synaptic plasticity beyond the boundaries that confine studies in which action potential based protocols are used. In addition to being able to precisely control calcium influx into presynaptic terminals, microelectrode access to presynaptic terminals allows one to manipulate the transmitter secretion process biochemically by injecting chemicals, peptides, and even proteins. Gaining biophysical and biochemical access to presynaptic terminals in a synapse exhibiting robust synaptic plasticity should provide a new venue for the investigation of synaptic plasticity.

In this report we examine the depolarization-release (D-R) coupling properties of the crayfish inhibitor. By correlating morphological and physiological parameters and by modeling, we identify optimal experimental conditions required to achieve consistent control of membrane potential in presynaptic terminals of the inhibitor.

METHODS

Animals and preparations

Crayfish (*Procambarus clarkii*) were obtained from Carolina Biological, Burlington, NC. The typical size of the animals was ~3.8 cm head to tail. The opener muscle of the first walking leg was used for all experiments. The propodite of the first walking leg was ~2.5 mm in length and 0.8 mm in width. Dissection of the preparation has been published before (Wojtowicz and Atwood 1984). The preparation was glued to the cover of a 35-mm petri dish and visualized through a Nikon SMZ-2B dissecting microscope, $\times 75 \sim \times 225$. A fiberoptic illuminator was mounted on a manipulator and the end of a fine plastic fiber was immersed in saline. The immersion prevented glare from surface reflection and the micropositioning ensured an optimal contrast for visualizing unstained axons. This optical setup allowed us to visualize thick tertiary branches but not varicosities in unstained preparations. The animals were maintained at room temperature, 21°C, until experiments, which were performed at 15°C.

Anatomy and electrophysiological arrangements

An example of the experimental configuration is shown in Fig. 1. The main branch of the inhibitor (1°), running along with the

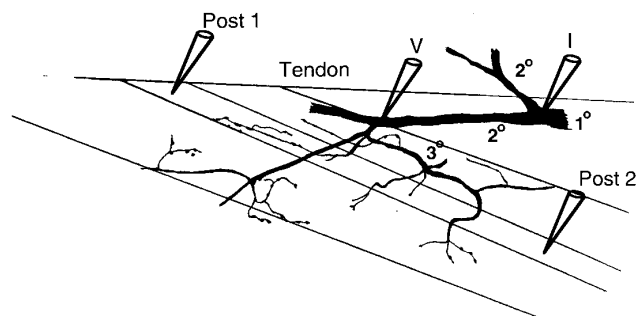


FIG. 1. Morphology of the crayfish neuromuscular junction and microelectrode placement. A partial morphological reconstruction of presynaptic branches is illustrated. Tendon and muscle fibers are drawn schematically but to scale. The locations of presynaptic voltage (V) and current (I) electrodes are marked. The I electrode is located at the Y branch point. The locations of the postsynaptic electrodes (Post 1 and Post 2) are marked. The primary, secondary, and tertiary axons are identified as 1°, 2°, and 3°, respectively. Scale bar: 50 μm .

excitor, bifurcates at the main branch point (Y branch point). Two presynaptic electrodes were used to impale the inhibitory axon. The presynaptic voltage electrode (V) always penetrated a secondary axon (2°), distal to the Y branch point, whereas the presynaptic current electrode (I) penetrated the Y branch point or the other side of the branch point. The V electrode was routinely placed 100–150 μm from the Y branch point. The V electrode approached the secondary branches with a shallow angle and was parallel to the branch. This electrode configuration facilitated axon penetration but did not allow the two electrode tips to be close to each other. The resulting separation compromised the speed of the voltage clamp and caused oscillatory transients at the onset and offset of voltage pulses. However, our goal was simply to control the membrane potential at the point of the presynaptic voltage electrode. No attempt was made to analyze the voltage-clamp current. Two postsynaptic electrodes (Post 1 and Post 2) penetrated a muscle fiber near the presynaptic voltage electrode. When the four-electrode arrangement was not possible we used only one electrode for postsynaptic recordings. The electrode placements around the Y branch point limited our recordings to central muscle fibers. A GeneClamp 500 (Axon Instruments) was used for presynaptic voltage control and two IE-201 intracellular amplifiers (Warner Instrument) were used to record from muscle fibers. Data were digitized with ITC-16Mac interface (Instrutech). Pulse Control, by Herrington and Bookman, University of Miami, was used for the control of data acquisition. Experimental data were typically filtered at 1.5–2 kHz and digitized at 10 kHz.

Morphological examination of investigated terminal branches was performed after electrophysiological recordings, by sketching or photography. The axons, both excitator and inhibitor, were stained with methylene blue, 1 mM for 7 min, or 4-Di-2-Asp (Molecular Probes), 5 mM for 2 min, to verify the origin and distribution of terminal branches on the muscle fiber studied. Sometimes Lucifer yellow was injected into the inhibitor for the same purpose.

Solutions

Dissection and the initial presynaptic electrode penetrations were conducted in a control saline composition, in mM: 195 NaCl, 5.4 KCl, 13.5 CaCl_2 , 2.6 MgCl_2 , and 10 sodium *N*-2-hydroxyethylpiperazine-*N'*-2-ethanesulfonic acid (NaHEPES), pH 7.4. After presynaptic electrode penetrations, the control saline was replaced by an experimental solution composition: 155 mM NaCl, 40 mM tetraethylammonium chloride (TEACl), 5.4 mM KCl, 10 mM CaCl_2 , 6.1 mM MgCl_2 , 10 mM NaHEPES, 1 mM 4-aminopyridine, and 300 nM tetrodotoxin, pH 7.4. The presynaptic voltage electrode

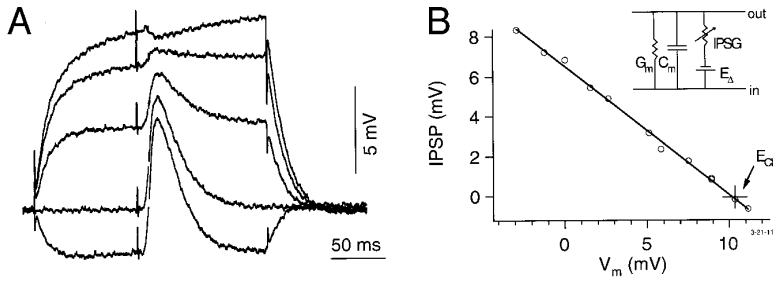


FIG. 2. Measurements of chloride equilibrium potential (E_{Cl}). *A*: inhibitory postsynaptic potentials (IPSPs) were activated by inhibitor action potentials that were timed 100 ms after the onset of current pulses used to change membrane potential of the muscle fiber. IPSP amplitudes are large here because the experiment was performed in the presence of 20 mM tetraethylammonium (TEA) and 1 mM 4-aminopyridine. *B*: plot of IPSP amplitude against membrane potential. Resting membrane potential is defined as 0 mV on the X-axis. E_{Cl} is 10 mV above the resting potential. *Inset*: circuit diagram representing the crayfish muscle fiber membrane and γ -aminobutyric acid (GABA)-mediated chloride conductance.

contained 1 M CsCl, 0.6 M TEACl, and 0.6 M KCl and had a resistance of 20 M Ω . Presynaptic current electrodes had resistances of 6–10 M Ω and contained 3 M KCl. Muscle electrodes contained 3 M KCl or 2 M CsCl and had resistances of 6–10 M Ω . All chemicals were purchased from Sigma unless otherwise indicated.

Chloride equilibrium potential

Given our electrode placement and electrode resistance, the noise level of postsynaptic current clamp, when presynaptic voltage clamp was turned on, allowed us to resolve inhibitory postsynaptic potential (IPSP) amplitudes of $\sim 200 \mu\text{V}$ after an average of three trials. This relatively high noise level was partly due to the current injected by the presynaptic voltage-clamp circuit. We found that simultaneous pre- and postsynaptic voltage clamp further reduced the postsynaptic signal-to-noise ratio. Furthermore, postsynaptic voltage clamp exaggerated transients associated with the onset and offset of presynaptic pulses, which complicated the measurement of IPSP amplitudes. However, current-clamp recording of IPSP does not always accurately reflect the quantity of transmitter release. The relationship between IPSP amplitude and transmitter release is not linear if the chloride driving force is small (Martin 1955). The crayfish muscle is known to control the intracellular chloride concentration efficiently and keep the chloride equilibrium potential (E_{Cl}) near its resting membrane potential (Finger and Stettmeier 1981). To correct for the resulting nonlinearity between IPSP amplitudes and the amount of transmitter that is released, E_{Cl} was measured whenever two-electrode postsynaptic recording was possible. Figure 2*A* illustrates an example in which IPSPs are recorded at different levels of membrane potential. The amplitudes of IPSPs decrease as membrane potential approaches E_{Cl} (Fig. 2*B*). Average chloride driving force (E_{Δ}), calculated as the difference between E_{Cl} and resting membrane potential, is 11.3 ± 4.0 (SD) mV ($n = 69$) and has a range of 5.2–26 mV. Typically, E_{Cl} was measured after each experimental protocol and up to 20 measurements were made in each preparation. E_{Cl} reached a steady state 5–10 min after a muscle fiber was penetrated and it remained stable, with a drift of $<5\%$, for ≥ 4 h.

In an effort to correct for the nonlinear summation of IPSPs, a circuit model for the crayfish muscle is constructed (Fig. 2*B*, *inset*). The circuit includes membrane conductance (G_m), membrane capacitance (C_m), and a variable Cl conductance (IPSG) with a chloride battery (E_{Δ}) arranged in parallel. This circuit does not take into account the spatial decay of the IPSP. However, this simplification is justified because synaptic varicosities on the crayfish neuromuscular junction are known to be widely distributed on the muscle surface and muscle fibers in small crayfish are known to have a long space constant (McLachlan and Martin 1981; Wojtowicz and Atwood 1986; and see below). The general equation describing current flow in the circuit is

$$C_m \frac{d\text{IPSP}(t)}{dt} + G_m \cdot \text{IPSP}(t) = \text{IPSG}(t) \cdot [E_{\Delta} - \text{IPSP}(t)] \quad (1)$$

where $\text{IPSP}(t)$ and $\text{IPSG}(t)$ represent IPSP and IPSG time courses. Arithmetic rearrangement of the equation gives rise to

$$\frac{\text{IPSG}(t)}{G_m} = \frac{\tau_m \cdot \frac{d\text{IPSP}(t)}{dt} + \text{IPSP}(t)}{E_{\Delta} - \text{IPSP}(t)} \quad (1A)$$

where $\tau_m (= C_m/G_m)$ represents the muscle fiber membrane time constant. For IPSP peak amplitudes ($\text{IPSP}_{\text{peak}}$), the derivative term of Eq. 1*A* becomes zero

$$\frac{\text{IPSG}_{\text{peak}}}{G_m} = \frac{\text{IPSP}_{\text{peak}}}{E_{\Delta} - \text{IPSP}_{\text{peak}}} \quad (2)$$

Multiplying both sides of Eq. 2 by the driving force gives rise to

$$\text{IPSP}_{\text{cor}} = \frac{i_{Cl}}{G_m} = \frac{\text{IPSP}_{\text{peak}}}{1 - \frac{\text{IPSP}_{\text{peak}}}{E_{\Delta}}} \quad (2A)$$

where i_{Cl} is equivalent to the chloride current recorded under voltage clamp. Equation 2*A* is identical to the formulation of Martin (1955), and IPSP_{cor} represents the corrected IPSP peak amplitude.

The circuit model and the equations assume a perfect space clamp of muscle fibers. Because of the long space constant of the muscle fibers and the relatively slow time course of the inhibitory postsynaptic current (IPSC), synaptic current can be recorded with a minimal distortion. Figure 3*A* illustrates IPSPs recorded, under current clamp, at two separate points in a muscle fiber (see *inset* for the relative positions of the electrodes V1 and V2 on the muscle fibers). The two IPSPs have identical amplitudes and time courses, suggesting isopotentiality of the muscle fiber. The muscle fiber was then voltage clamped by two-electrode voltage clamp (see Fig. 3*B*, *top trace*, for IPSC). The “unclamped” synaptic potentials are $<2\%$ of the IPSP amplitudes recorded under current clamp (Fig. 3*B*, *bottom traces*). Therefore the IPSC recorded in muscle fibers provides an accurate estimate of the synaptic current.

Because it is possible to convert IPSP into IPSG with the use of Eq. 1*A*, together with measurements of τ_m , G_m , and E_{Δ} , one can verify the circuit model and Eq. 2*A* by comparing the IPSG time course with that of IPSCs measured under voltage clamp. Figure 4*A* illustrates a comparison of an IPSP (—) and an IPSG ($\cdot \cdot \cdot$) converted from the IPSP. The IPSG exhibits a faster time course than that of IPSP because the effect of muscle C_m has been corrected for. The conductance was then multiplied by the driving force to obtain an expected IPSC [Fig. 4*B*, $\cdot \cdot \cdot$, which closely approximates the time course and amplitude of the voltage-clamped IPSC (Fig. 4*B*, —)]. Tests performed in 10 preparations consistently demonstrated a close match between the time courses of the IPSC and IPSG. The validity of the circuit model and Martin’s correction procedure for IPSP peak amplitudes is therefore verified. Furthermore, the matching also suggests that we can extract the IPSG time course from the IPSP waveform if E_{Cl} , G_m , and τ_m are measured.

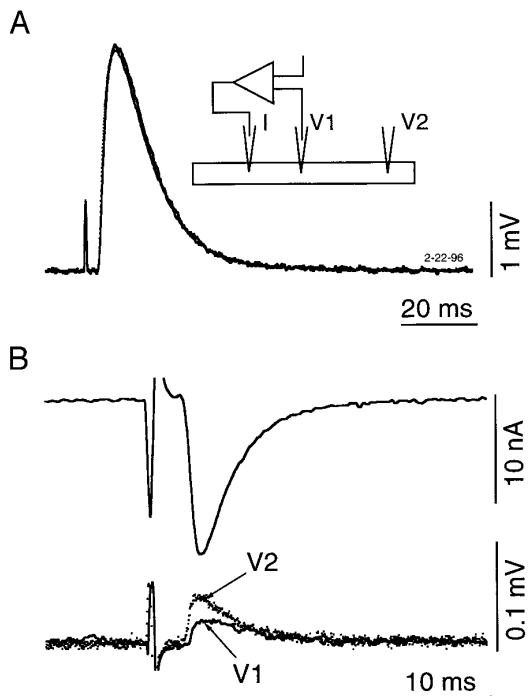


FIG. 3. Space clamp of muscle fibers. *A*: superimposed IPSPs recorded from microelectrode 1 (V1) and microelectrode 2 (V2) of the same muscle fiber under current clamp. Microelectrodes V1 and I were used for voltage clamp. The separation between V1 and V2 is roughly $250\ \mu\text{m}$. The 2 recordings exhibit an identical IPSP amplitude and time course. *B*, top trace: inhibitory postsynaptic current (IPSC) recorded from the same muscle shown in *A*. *B*, bottom traces: "residual IPSPs" recorded from V1 (—) and V2 (· · ·) during voltage clamp. The amplitudes of the residual IPSPs are $<2\%$ of those recorded under current clamp. Transmitter release was evoked by inhibitor action potentials and in the presence of 20 mM TEA and 1 mM 4-aminopyridine. The current trace shown in *B* was filtered at 500 Hz. All of the traces in *B* are averages of 50 trials.

RESULTS

D-R coupling relationships

Examples of recordings from a D-R coupling protocol are shown in Fig. 5*A*, where both presynaptic (*A2*) and postsynaptic (*A1*) recordings are illustrated. Presynaptic pulses of 5 ms were used for most of our studies. Increasing the amplitude of presynaptic pulses causes a graded increase in IPSP amplitudes. The D-R coupling curves of IPSP_{cor} and the integral of IPSC converted from IPSP ($\text{IPSG}_{\text{area}}$) measured from the same synapse are both plotted in Fig. 5*B*. The threshold of transmitter release at this synapse is about $-35\ \text{mV}$ and the IPSP_{cor} reaches its maximal level at $-10\ \text{mV}$. A clear suppression is observed with larger

depolarizations. In 12 preparations, the thresholds of transmitter release varied from -30 to $-40\ \text{mV}$ and their maximal levels were typically reached at -10 – $0\ \text{mV}$. Composite IPSP_{cor} s (open symbols) and $\text{IPSG}_{\text{area}}$ s (filled symbols) from three additional experiments are shown in Fig. 5*C*. (The remaining 8 preparations are not shown because E_{Cl} was not measured.) The identical shapes of the D-R coupling curves measured from the IPSP_{cor} and $\text{IPSG}_{\text{area}}$ suggest that both parameters are equally valid as a measurement of total transmitter release.

Total transmitter release is mediated by two components of calcium influx activated by a depolarizing pulse: the ON current (IPSP_{on}), activated during the pulse, and the tail current (IPSP_{off}), which occurs at the end of the pulse. To evaluate the control of presynaptic potentials during a presynaptic pulse, it would be necessary to measure transmitter release activated by the ON current. Under our experimental conditions, transmitter release activated by 5-ms pulses rarely starts during the pulse; the measurement of IPSP_{on} has to be made after the end of 5-ms pulses. To avoid contamination of IPSP activated by the tail current, the synaptic delay of IPSP_{off} has to be measured first. Figure 6*A* shows three traces in which transmitter release during the 10-ms presynaptic pulses was suppressed by progressively larger pulses. An IPSP_{off} is clearly identifiable when transmitter release is completely suppressed during the pulse (dotted curves). (The slightly higher baseline of the dotted curve during the presynaptic pulse is an artifact.) Synaptic delay activated by tail current, measured from the termination of the presynaptic pulse to the onset of the IPSP (arrow), is 2.75 ms in this example. In 4 preparations where IPSP_{off} is clearly identified, synaptic delay ranged from 2 to 2.9 ms ($2.5 \pm 0.4\ \text{ms}$). [The estimate of synaptic delay is long relative to that of the squid giant synapse (Augustine et al. 1985a; Llinás et al. 1981b). The longer delay here could be due to the experimental temperature, 15°C , which was significantly lower than that which the animals had acclimated to, 21°C . The difference could also be partially attributed to the long membrane time constant of the crayfish opener muscle fibers ($13.0 \pm 3.8\ \text{ms}$, $n = 30$), which may slow the rate of rise of IPSPs and delay the detection of IPSPs above noise level. These factors also explain why we rarely observed detectable IPSPs during 5-ms pulses. Significant release during the 5-ms pulse could be routinely detected during facilitation or at 21°C (data not shown)].

The D-R coupling curve of IPSP_{on} , mediated by 5-ms pulses, was measured from an experiment illustrated in Fig. 6*B*. Although the transmitter release or suppression during the 5-ms pulses is not obvious, it is clear that the largest depolarization

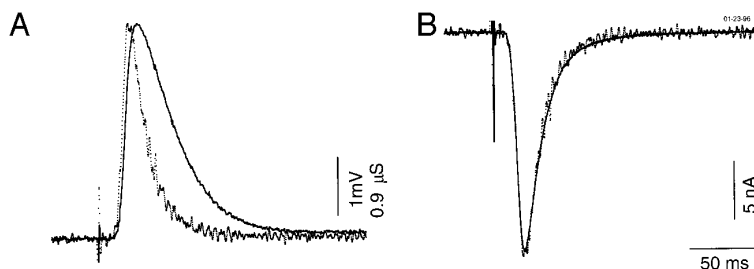


FIG. 4. Comparison of IPSP, IPSC, and IPSG. *A*: IPSP (—) and IPSG (· · ·) converted from the IPSP. The τ_m , membrane resistance, and chloride driving force (E_{Cl}) of the muscle fiber used to calculate IPSG by Eq. 1*A* are 10 ms, $0.35\ \text{M}\Omega$, and 5.8 mV, respectively. *B*: IPSC (—) recorded under voltage clamp has identical amplitude and time course to that estimated from IPSG and the chloride driving force (· · ·). Transmitter release was triggered by presynaptic action potentials and in the presence of 20 mM TEA and 1 mM 4-aminopyridine. The IPSC and IPSP are averages of 50 trials.

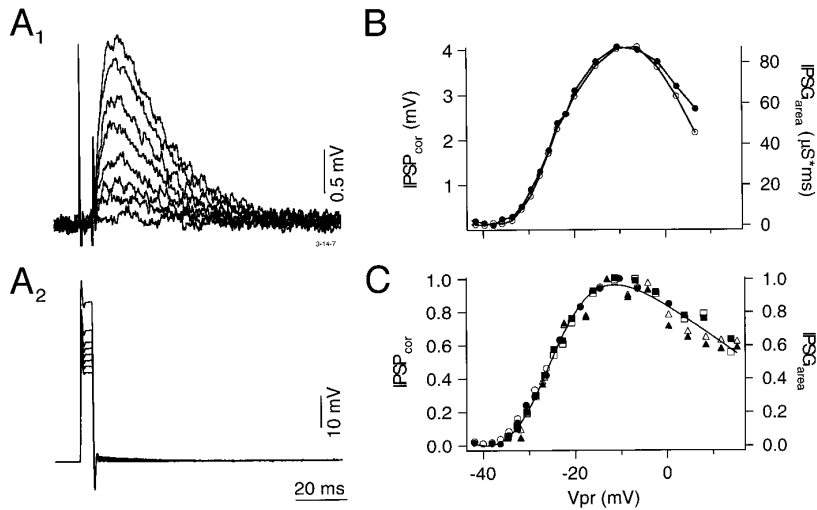


FIG. 5. Depolarization-release (D-R) coupling plot of the crayfish inhibitor. *A*: presynaptic (*A2*) and postsynaptic (*A1*) recordings of an inhibitor. The presynaptic holding potential is -65 mV. The E_{Δ} in this preparation is 5.2 mV. *B*: D-R coupling curves of corrected IPSP peak amplitude ($IPSP_{cor}$) (\circ) and the integral of IPSP converted from IPSP ($IPSG_{area}$) (\bullet). The 2 measurements yield virtually identical D-R coupling curves. *C*: composite of D-R coupling plots from 3 preparations. All of the D-R coupling plots are normalized to a maximum of 1. Open symbols: $IPSP_{cor}$ s. Filled symbols: $IPSG_{area}$ s. Thresholds of release in these experiments are not identical; therefore the X-axis is shifted by $2 \sim 3$ mV to achieve optimal alignment. The smooth curve is drawn by hand. *B* and *C* share the same X-axis. Vpr: level of presynaptic depolarization measured by averaging the potential from the 3rd to the 5th ms of 5-ms pulses.

(dotted curve) can suppress transmitter release. Because the average synaptic delay of $IPSP_{off}$ is 2.5 ms, $IPSP_{on}$ is measured at this point (Fig. 6*B*, arrow). The D-R coupling plot of $IPSP_{on}$ is shown in Fig. 6*C*. The suppression of $IPSP_{on}$ is more pronounced than that measured from $IPSP_{cor}$. This suppression is a consistent finding, and a composite of D-R coupling plots from nine preparations is shown in Fig. 6*D*. The smooth curves in Fig. 6, *C* and *D*, are derived from the D-R coupling plot of the squid giant synapse (Smith et al. 1985). We did not correct for the nonlinear summation of $IPSP_{on}$ because Martin's equation is only valid for peak amplitudes. One can theoretically perform such measurements on converted IPSPs. However, the conversion was not performed in every preparation because of difficulties in measuring E_{Cl} routinely. Fortunately, the maxi-

mal amplitude of $IPSP_{on}$ was generally in the range of 10–20% of the maximal IPSP peak amplitudes. The effects of nonlinear summation in this range should consequently be minimal (McLachlan and Martin 1981).

Physiological and morphological correlation of the inhibitor

The D-R coupling curves shown in Figs. 5 and 6 were obtained from preparations in which morphological arrangements were optimal, namely, the muscle fiber under study was innervated by a single tertiary branch originating from a point near the presynaptic voltage electrode. A common complication we encountered was that muscle fibers were

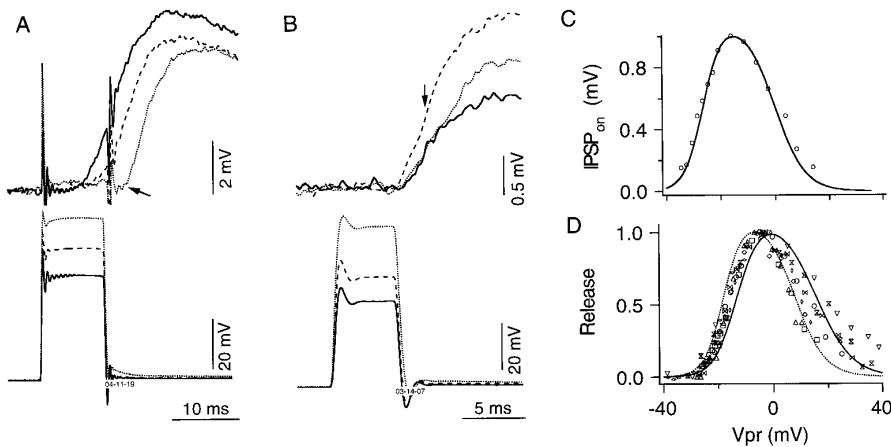


FIG. 6. Suppression of transmitter release at the crayfish inhibitor. *A*: $IPSP_{off}$ is identified when transmitter release is completely suppressed during presynaptic pulses. Pre- and postsynaptic responses of 10-ms pulses are shown. Line styles of pre- and postsynaptic traces are matched. When the presynaptic pulse is depolarized to $+60$ mV (dotted curve) there is no release during the 10-mV pulse while the $IPSP_{off}$ takes off 2.75 ms after the termination of the pulse (arrow). *B*: simultaneous pre- and postsynaptic recordings to illustrate suppression of transmitter release mediated by 5-ms presynaptic pulses. The trace styles are matched for pre- and postsynaptic recordings. Artifacts associated with the onset and offset of presynaptic pulses are removed. Arrow: point where the $IPSP_{on}$ is measured. Traces in *A* are obtained from a different preparation than those in *B*. *C*: D-R coupling of $IPSP_{on}$ measured, at 2.5 ms after the end of presynaptic pulses, from the same preparation as shown in *B*. The smooth curve is adapted from the D-R coupling plot of the squid giant synapse (Smith et al. 1985). *D*: composite of D-R coupling plots from 9 preparations. The maximal level of each experiment is normalized to 1. X-axes of some experiments were horizontally shifted to achieve optimal alignment. Dotted curve: D-R coupling curve of the squid giant synapse. Solid curve is calculated from the same synapse but its terminal has a space constant 8 times longer than its own length (see legend to Fig. 8). *C* and *D* share the same X-axis.

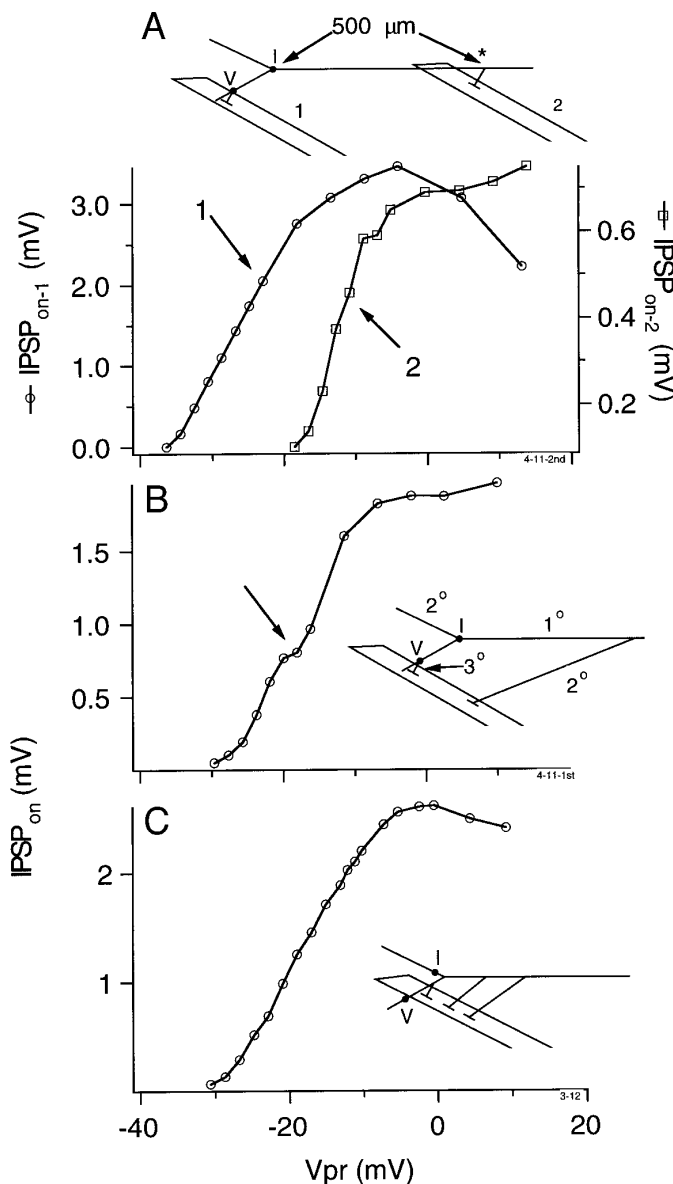


FIG. 7. Morphological and physiological correlation. *A*: D-R coupling curves of $\text{IPSP}_{\text{on-1}}$ recorded from 2 separate muscles. Recordings from muscle fiber 2 exhibit a steep rising phase and a much higher threshold. The location of presynaptic voltage (V) and current (I) electrodes is identified. The distance between the Y branch point, I , and the point of origin of the distant fiber ($*$) is $\sim 500 \mu\text{m}$. *B*: D-R coupling plot of a muscle fiber innervated by 2 widely separated branches. The step on the rising phase (\downarrow) of the D-R coupling plot is presumably mediated by the distant branch. The primary, secondary, and tertiary branches are labeled 1° , 2° , and 3° , respectively. *C*: D-R coupling plot of a multiply innervated muscle fiber with clustered points of origin. The rising phase of the curves looks normal but there is very little suppression. Details of terminal arborization are not shown, but the positions of presynaptic electrodes and branching patterns of primary, secondary, and tertiary branches are drawn to scale. All of the D-R coupling curves were measured from IPSP_{on} . *A*–*C* share a common X-axis.

sometimes innervated by more than one branch, one of which originated from a distant point. To illustrate the effect of a distant branch, we recorded from two widely separated muscle fibers, each innervated by a single presynaptic branch (Fig. 7*A*). Muscle fiber 1 is innervated by a branch near the presynaptic voltage electrode and its D-R coupling plot,

constructed from IPSP_{on} , exhibits a bell shape (\circ). However, recordings from muscle fiber 2, which is innervated by a distant branch, give rise to a higher release threshold, a steep rising phase, and no suppression. In preparations in which a muscle fiber is innervated by multiple branches with widely separated origins (Fig. 7*B*), the D-R coupling plot exhibits the combined characteristics of near and distant branches. There is a step on the normal rising phase (\downarrow) and there is no suppression. The steep rising phase, the absence of suppression and the step observed in the two examples suggest that transmitter release was activated by an uncontrolled calcium spike in the distant branches. A less extreme example is shown in Fig. 7*C*, where the muscle fiber is innervated by multiple branches but their points of origin are not widely separated. In this case, the D-R coupling curve does not show a steep rising phase but there is little suppression of transmitter release, suggesting an anisopotentiality of presynaptic terminals. (See below). In all cases in which a clear suppression of transmitter release is observed in the D-R coupling plot of IPSP_{cor} or IPSP_{on} , the recorded muscle fibers were innervated singly by a branch originating within 50–100 μm of the presynaptic voltage electrode.

Table 1 summarizes the impact of axonal morphology and electrode placement on D-R coupling plots. Although detailed arborizations of the inhibitor on muscle fibers are highly variable, we found that the shapes of the D-R coupling plots mainly correlated with the patterns of major branches. Placement of presynaptic voltage electrodes in the primary branch (1st column) invariably failed to control potentials in terminal branches regardless of the positions of the muscle fibers we studied. With presynaptic voltage and current electrodes in separate secondary branches (2nd column), control also invariably failed in multiply innervated muscle fibers. In singly innervated muscle fibers, control was variable in that one could sometimes but not always achieve fair control of release sites and suppress release. Finally, the best configuration is to place the presynaptic voltage electrode in a secondary branch while the current electrode penetrates the Y branch point (3rd column). Clear suppression of transmitter release with a consistent shape of the D-R coupling curve can be obtained in all singly innervated muscle fibers, whereas suppression is achieved only occasionally in multiply innervated ones.

Effects of space clamp on the D-R coupling curve

Thus far, the presence of suppression has been used as an indicator of the quality of presynaptic voltage control. We further explore the correlation between presynaptic isopotentiality and suppression of transmitter release by constructing a model. Terminal arborizations of an inhibitor are approximated by a single cable with a length of 1 and with a uniform distribution of release sites. Point 0 of the cable is equivalent to the location of the presynaptic voltage electrode (Fig. 8*A*, diagram). The spatial decay of presynaptic depolarizations is approximated by a single exponential decay with a range of space constants from 0.25 to 8. Assuming a holding potential of -70 mV , the presynaptic potential along the cable should be represented as

$$V_{\text{pr}}(x) = -70 + A * e^{-x/\lambda} \quad (3)$$

TABLE 1. Correlation between morphology and D-R coupling curves

	V Electrode In 1° Branch	V and I Electrodes in Different 2° Branches		V Electrode in 2° Branch, I Electrode at the Y Branch Point	
Morphology and electrode arrangements					
	13	2	0	4	0
	7	0	2	7	0
	0	0	3	3	11

The distance between presynaptic V electrodes from the Y branch point, 2nd and 3rd columns, is $\sim 100\text{--}150\ \mu\text{m}$. D-R, depolarization-release. The criteria for spiking and suppression are based on D-R coupling plots constructed from IPSP_{on} . Values are number of preparations observed under each category.

where $V_{\text{pr}}(x)$ represents the peak level of a presynaptic pulse at point x , A represents the absolute amplitude of a presynaptic depolarization recorded by the presynaptic voltage electrode, and λ represents a space constant. Figure 8A illustrates the spatial decay of a presynaptic pulse depolarized to 0 mV at point 0 for three cables with the indicated space constants.

To evaluate transmitter output along the cable, we divide the cable into 100 equal compartments and the level of transmitter output of each compartment is determined from the D-R plot of the squid giant synapse (squid template) (Fig. 8C, \square and dotted line). (The squid data were adapted from Fig. 2 of Smith et al. 1985.)

The spatial profiles of transmitter release along four cables, $\lambda = 0.25, 1, 2,$ and 8 , are illustrated in Fig. 8B when point 0 is depolarized to 0 mV. It is clear that transmitter release is restricted to the proximal end for the cables with short space constants. A comparison between the spatial profile of presynaptic potential (Fig. 8A) and that of release (Fig. 8B) indicates that the steep D-R coupling curve of the squid template is responsible for the more severe spatial nonuniformity of transmitter release. We further calculate total transmitter output of the cable by summing the release calculated from each compartment. The sum is then normalized by the total release of a cable with an infinite space constant. The D-R coupling curves of the cables with different space constants are shown in Fig. 8C. Given the range of depolarization we have considered, suppression of neurotransmitter release

is only predicted for cables with a space constant >2 , because one cannot suppress release of an entire cable unless most release sites are depolarized beyond their maximal point of the D-R coupling curve. For a cable with a space constant of 8, spatial profiles of transmitter release at several levels of presynaptic depolarization are illustrated in Fig. 8D. The nonuniformity of release occurs at all levels. The relative nonuniformity in release is more pronounced than that of presynaptic potentials because of the steep D-R coupling relationship.

To establish a quantitative correlation between presynaptic space constant and the extent of transmitter suppression, we plot the half-width of the D-R coupling curve against the space constant in Fig. 8E. The half-width narrows as the space constant increases. The right axis indicates that terminals with a space constant of >4 would give rise to a half-width within 20% of that of an infinitely long cable (---).

The D-R coupling relationship of the squid giant synapse shown in Fig. 8C was obtained from postsynaptic recordings measured within the duration of 6-ms presynaptic pulses (Smith et al. 1985). This measurement estimates release activated by ON current, which is comparable with the IPSP_{on} shown in Fig. 6, C and D. The D-R coupling curve shown in Fig. 6C shows a near-perfect match between a crayfish inhibitor preparation and the squid template with an infinitely long space constant. The dotted curves shown in Fig. 6D are calculated from a cable with an infinitely long space constant, whereas the solid line represents the D-R plot of a

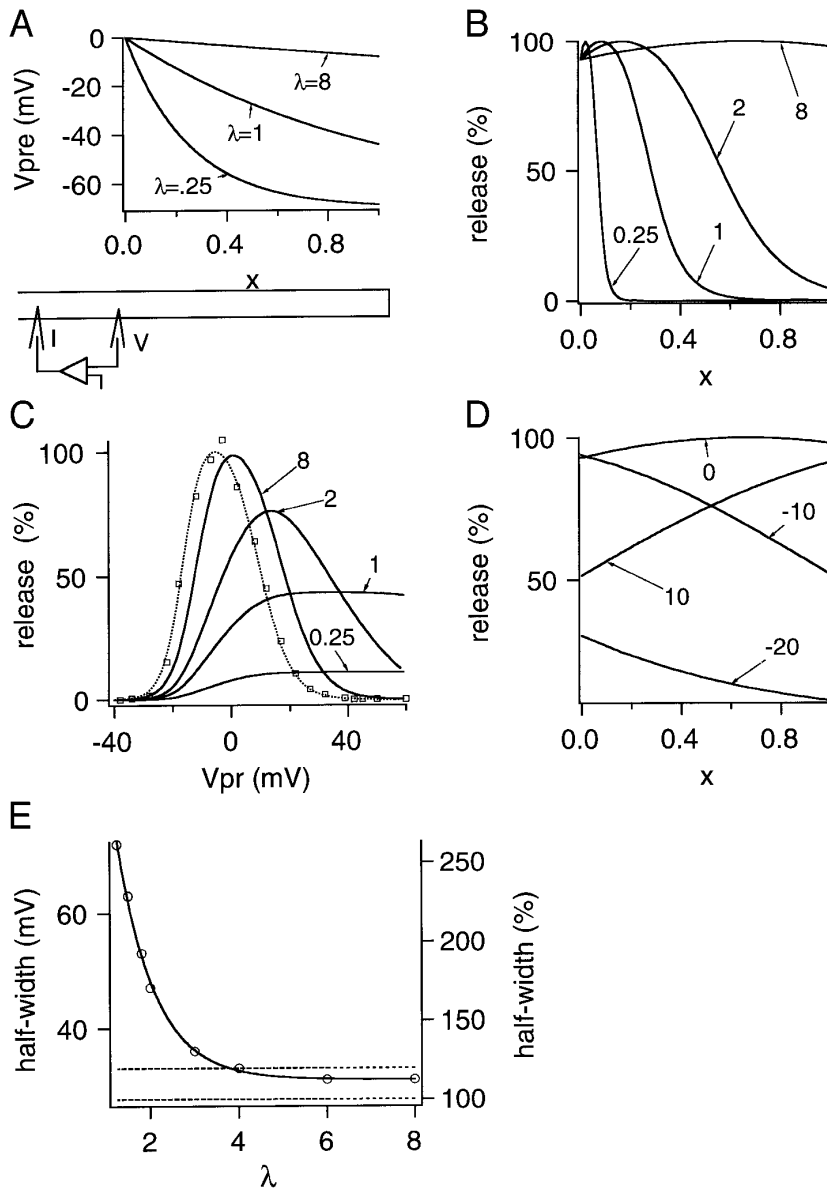


FIG. 8. Modeling of the effects of presynaptic spatial control on the depolarization response coupling plot. *A*: spatial decay of a presynaptic pulse in 3 cables with space constants of 0.25, 1, and 8, respectively. The presynaptic pulse is depolarized to 0 mV at point 0, from a holding potential of -70 mV. Diagram: location of the presynaptic voltage electrode is equivalent to point 0. *B*: spatial profile of transmitter release for 4 cables with $\lambda = 0.25, 1, 2,$ and 8. Release is activated by a pulse depolarized to 0 mV at $x = 0$. Each cable is divided into 100 equal compartments, and the release level for each compartment is determined directly from the squid template shown in *C*. *C*: D-R coupling plot of the squid template, dotted line fitted to the squid data (\square), and a family of cables with indicated space constants. The release for a cable at a particular depolarization level was calculated as the sum of releases from all compartments of the cable. This sum was then normalized to the release of a cable with an infinitely long space constant. *D*: spatial profile of transmitter release for a cable with a space constant of 8. Lines: release profiles activated by pulses depolarizing the head of the cable to the potentials indicated. *E*: relationship between the half-width of the D-R coupling curve and the space constant. The data are also normalized to the half-width of the squid template (right axis). Cables with a space constant 4 times longer than their physical lengths have half-width values within 20% of that of an infinitely long cable.

cable with a space constant of 8. The two curves “envelope” $>90\%$ of the data points measured from the crayfish inhibitor. (The squid curves were shifted horizontally to be aligned with the crayfish data in Fig. 6, *C* and *D*.) Finally, in preparations in which muscle fibers were innervated by multiple branches, the D-R coupling curve exhibits a long rising phase and shows little suppression (Fig. 7*C*), which is similar to the model cable with a space constant of 2. Assuming that the shape of the D-R coupling curve is a realistic indicator of presynaptic space clamp and that the crayfish inhibitor D-R coupling characteristics are similar to those of the squid giant synapse, our model suggests that presynaptic isopotentiality of the crayfish inhibitor is equivalent to a cable with a space constant ≥ 8 times longer than its physical length.

Effects of presynaptic pulse duration on transmitter release

Presynaptic voltage control offers a large degree of freedom in the waveform of the presynaptic pulse. We explored

the effect of presynaptic pulse duration on transmitter release to find an optimal combination of parameters for our study. In addition, a comparison between IPSPs activated by action potentials with those activated by presynaptic pulses with action-potential-like waveforms should provide further information for the evaluation of presynaptic space clamp. Examples of IPSPs activated by presynaptic pulses of different durations are illustrated in Fig. 9*A*. The 2-ms pulse activates an IPSP of 0.08 mV, which is barely above the background noise level (*top trace*). The 20-ms pulse ($\cdot \cdot \cdot$) appears to nearly saturate the release machinery, because it activates an IPSP that is only slightly larger than that activated by the 10-ms pulse (---). (If the nonlinear summation is corrected, the IPSP activated by the 20-ms pulse will be 36% larger than that activated by the 10-ms pulse.) Figure 9*B* shows the D-R coupling plots constructed from pulses of different durations recorded from a different synapse. Both the peak amplitudes of IPSPs and the thresholds of release are dependent on presynaptic pulse duration. The

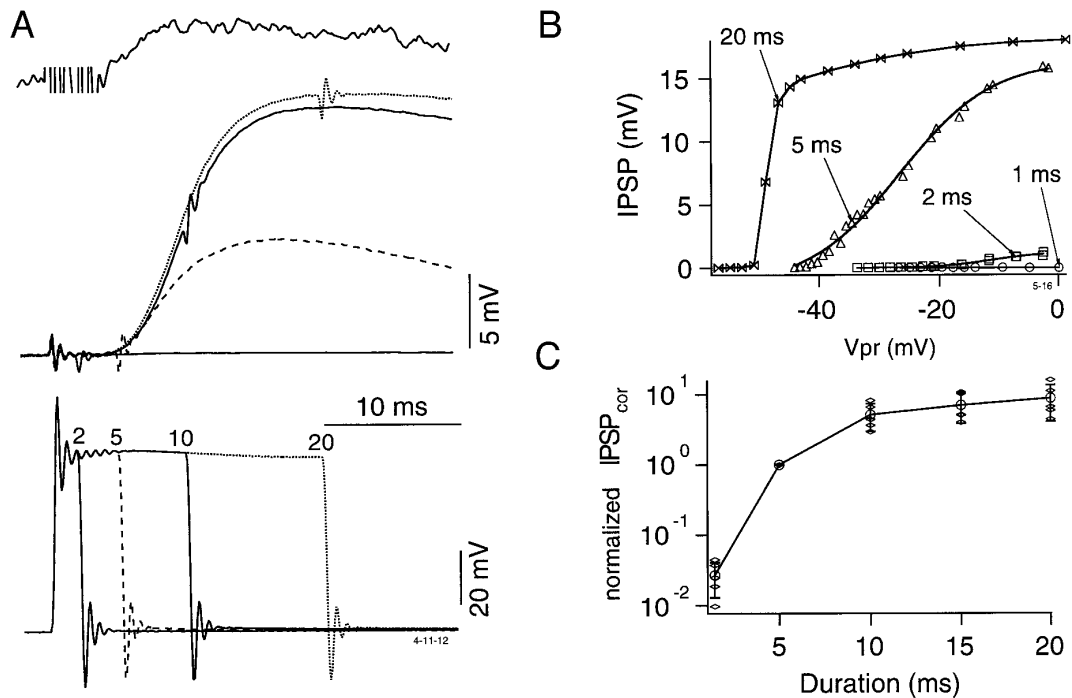


FIG. 9. Effects of presynaptic pulse duration on neurotransmitter release. *A*: pre- and postsynaptic recordings to illustrate the effects of presynaptic pulse duration on the amount of transmitter release. The trace patterns of pre- and postsynaptic recordings are matched. *Top trace*: IPSP activated by the 2-ms pulse at a high amplification. This trace is an average of 20 trials. Transients associated with the presynaptic pulse are erased. *B*: D-R coupling of presynaptic pulses of different durations. All of the recordings were obtained from the same preparation. The nonlinear summation of IPSP peak amplitudes (IPSP_{peak}) was not corrected for. The duration of presynaptic pulses affects both release threshold and IPSP amplitude. *C*: effect of presynaptic pulse duration on transmitter release. All of the IPSP_{cor}s were normalized to those activated by 5-ms pulses. Presynaptic pulses were depolarized to 0 mV. Each data point, except for the 5-ms point, is averaged from 5 preparations, and SDs are also shown. Individual data points are also plotted to show the extent of data scattering. Because we only examined 3 or 4 durations in each preparation, the graph is pooled from experiments performed on 9 preparations.

threshold of transmitter release becomes more negative as the presynaptic pulse duration is increased. The precise release thresholds for the 1- and 2-ms pulses are difficult to establish, because the IPSP amplitudes are barely above background noise level. The extremely negative threshold and steep rising phase of the D-R coupling curve mediated by 20-ms pulses have been observed before and might be due to a facilitated transmitter release primed by a small calcium influx during the small but long-lasting depolarization (Wojtowicz and Atwood 1984). [The lack of suppression in the D-R coupling plot of the 5- and 20-ms pulses in Fig. 9*B* is mainly due to the fact that the *Y*-axis represents uncorrected IPSP peak amplitudes. D-R coupling curves constructed from such measurements exhibit a less apparent suppression. In the case of the D-R coupling curve mediated by 20-ms pulses, the main factor contributing to the lack of suppression is that the small pulses have already released nearly all the available vesicles and larger depolarizations could not further increase release. In addition, the maximal level of IPSPs activated by 20-ms pulses are approaching E_{Cl} , a situation that further compresses the differences of IPSP peak amplitudes. IPSP_{on} measured from the same synapse exhibits clear suppression (data not shown).]

The relationship between IPSP_{cor} and presynaptic pulse duration, for presynaptic pulses depolarized to 0 mV, is illustrated quantitatively in Fig. 9*C*. Transmitter release activated by a 1- to 2-ms pulse is barely detectable, whereas IPSPs

activated by 20-ms pulses approach a plateau level. (IPSPs activated by 1- and 2-ms pulses are combined in the average of the 1st data point). With the use of 2-ms presynaptic pulses depolarized to 0 mV to approximate the waveform of an action potential at 15°C, the average IPSP amplitude is $108 \pm 56 \mu V$ ($n = 5$), which is similar to the averaged responses activated by action potentials, $50 \pm 40 \mu V$ ($n = 21$). We choose 5-ms pulses to perform most of our experiments to obtain a good signal-to-noise ratio while remaining ~ 1 order of magnitude below the saturation level reached by 20-ms pulses.

DISCUSSION

In this report we characterize the D-R coupling relationship of the crayfish inhibitor. Analysis of E_{Cl} and IPSCs recorded in opener muscle fibers validates a procedure for correcting nonlinearity between IPSP amplitudes and transmitter release. Morphological and physiological correlation indicates that both the electrode placements and the branching pattern of inhibitors are important for achieving good presynaptic voltage control. The shape of D-R coupling curves and the cable-release model suggest that the voltage control technique is able to depolarize terminal branches near a presynaptic voltage electrode with a good spatial uniformity and without uncontrolled spikes. Analysis of the effects of pulse duration on transmitter release suggests that

5-ms presynaptic pulses are able to activate transmitter release over a wide range without saturating the release machinery.

This report establishes basic characteristics of D-R coupling and the extent of presynaptic voltage clamp at the crayfish inhibitor. This preparation is uniquely suitable for the study of synaptic facilitation for several reasons. First, the crayfish inhibitor exhibits a robust facilitation (Atwood and Bittner 1970; Dudel and Kuffler 1961a). Second, the presynaptic control method is particularly suitable for experimental protocols needed for the analysis of facilitation. To monitor facilitation, one typically compares transmitter release, triggered by a test pulse, before and after facilitation is activated. Such comparison, although requiring one important assumption, can keep several compounding problems in check. The assumption is that the presynaptic space constant is not changed during facilitation. If the assumption is verified, the imperfections in presynaptic space clamp will remain a constant factor for quantitative analysis of synaptic facilitation. One of the possible complicating factors of our method is that a prolonged depolarizing pulse may activate facilitated release during the pulse (Wojtowicz and Atwood 1984). This complication can be minimized if one restricts experimental protocols to 5-ms pulses. Furthermore, the comparison of control and facilitated responses can minimize this complication, if not correct for it completely. Finally, although our experimental configuration does not allow us to analyze presynaptic calcium currents, the calcium influx can be estimated by two methods. First, calcium imaging techniques have long been applied to the crayfish opener muscle (Delaney et al. 1989). The imaging of intracellular calcium concentration provides an indirect estimate of calcium influx activated by presynaptic activities. Second, the amplitudes of IPSPs, after the nonlinear summation is corrected for, can be used as an indicator of presynaptic calcium influx. For example, IPSP amplitudes activated by conditioning stimulations would allow us to establish a quantitative relationship between the calcium influx and the magnitude of synaptic facilitation. In short, given the constraints discussed in this paper, the presynaptic voltage control method in the inhibitor should enable valuable advances to be made in the study of synaptic plasticity.

Spatial control of presynaptic branches

It is important to emphasize that our presynaptic voltage control is mostly achieved in the area near to presynaptic voltage and current electrodes. Potentials in synapses located at some distance from the presynaptic electrodes are not controlled for two reasons. First, the diffusion of potassium channel blockers from the presynaptic voltage electrode is probably limited and the block of potassium channels in distant branches is less complete than in near branches. Second, a finite space constant of the presynaptic axon would preclude control of potential over an extended distance. As a result, presynaptic voltage-clamp current is not analyzed because it is generated from an extended area of the presynaptic axon where membrane potential is not uniform.

A cable-release model was constructed to evaluate the extent of spatial control of presynaptic potential in our preparation. The main assumption of the model that requires dis-

cussion is the use of the squid data for our modeling. This approach is justified for the following reasons. Calcium channels believed to be involved in neurotransmitter secretion are mainly N and P types (Dunlap et al. 1995; Mintz et al. 1995; Wu and Saggau 1994). The two types of calcium channels are kinetically very similar to each other (Lorenzon and Foehring 1995). The similarities in kinetics are also apparent when one compares the currents across species, from squid (Augustine et al. 1985b; Llinás et al. 1981a) to crayfish (Hong and Lnenicka 1995) and mammals (Lorenzon and Foehring 1995). Furthermore, pharmacological profiles of calcium channels involved in synaptic transmission are also similar across species (Araque et al. 1994; Grossman et al. 1991; Mintz et al. 1995; Wu and Saggau 1994). Allowing for some variation in the activation threshold, one cannot distinguish the species origin or the type of calcium current (I_{Ca}) by current-voltage curves or current waveforms. The current-voltage curve of I_{Ca} and the calcium cooperativity of the release process determine the shape of the D-R coupling curve (Augustine et al. 1985a; Lando and Zucker 1994; Llinás et al. 1981b). The current-voltage characteristics of the I_{Ca} recorded from crayfish motoneurons or the excitor of the opener muscle appear to be similar to those of a typical N- or P-type calcium current (Hong and Lnenicka 1995; Wright et al. 1994). Therefore, allowing for variation in the I_{Ca} activation threshold, the D-R coupling curve of the squid giant synapse is a reasonable reference.

The second simplification of the model that requires further discussion is the use of a simple exponential function to approximate the space constant. The main purpose of the model is to correlate the presence of suppression with the extent of isopotentiality. Variations in details of the spatial profiles of presynaptic potential decay should not significantly change the correlation. Similarly, the correlation between the presynaptic space constants and D-R coupling curves of transmitter release should be valid regardless of small variations in calcium channel kinetics or spatial profiles of potential decay. An analysis of passive cable properties of excitor axons has been carried out in crayfish under physiological conditions (Wojtowicz and Atwood 1984). We decided not to take the same approach because our experiments were performed in the presence of high levels of K^+ channel blockers, which renders the original passive model inapplicable.

Finally, we have used only one space constant for the entire presynaptic depolarizing range. Although this is certainly a simplification, we believe that there are minimal changes in the space constant as the level of depolarization varies. For example, the space constant may increase with large depolarizations if uncontrolled calcium spikes were generated in presynaptic branches. However, our morphological and physiological correlation suggests that D-R coupling curves associated with calcium spikes should exhibit no suppression and a steep rising phase (Fig. 7, *A* and *B*; unpublished observations). The presence of a gradual rising phase and suppression in the D-R plots implies that all of the release sites could be depolarized to desired levels without triggering uncontrolled spikes. At the other extreme, one could argue that the apparent suppression of IPSP was due to a severe decrease in the space constant activated by large presynaptic pulses, which would in turn restrict release to

proximal varicosities. This is unlikely, because we could achieve complete suppression during large presynaptic depolarizations with 10 ms pulses (Fig. 6A). If the suppression we observed had been due to transmitter release restricted to proximal varicosities, we would not have been able to suppress release completely during a long pulse because some of the varicosities would be in a release range as the presynaptic potential decayed along a terminal branch (Fig. 8, B and C, $\lambda = 0.25$ and 1). Furthermore, the detection of transmitter suppression is more consistent as we lower experimental temperature and $[Ca^{2+}]_o$, conditions that lengthen space constants by increasing membrane resistance (Thompson et al. 1985) and decreasing the activity of calcium-activated potassium current (Sivaramakrishnan et al. 1991). Consistent morphological and physiological correlation lends further support to the suggestion that suppression of transmitter release in the inhibitor is indeed due to a smaller calcium influx associated with large presynaptic depolarizations. In addition, studies of the crayfish excitor have indicated that the excitor terminal branches are electrotonically compact in physiological saline and in the presence of potassium channel blockers (Sivaramakrishnan et al. 1991; Wojtowicz and Atwood 1984). Because the inhibitor has a larger diameter than the excitor, it would have an even longer space constant (Florey and Cahill 1982; unpublished observations). Finally, the D-R coupling characteristics reported here are consistent with the basic features of a plot in which the voltage dependence of calcium influx was estimated from a current-clamp study of the crayfish excitor (Blundon et al. 1995). Therefore consideration of basic cable properties and several lines of independent experimental evidence supports the notion that a drastic change of space constant associated with different levels of depolarization is unlikely.

If the squid template and our cable-release model are realistic approximations to the crayfish inhibitor, it would then suggest that the inhibitor branches on central muscle fibers have a space constant of ≥ 8 times longer than their physical length in the presence of intra- and extracellular potassium channel blockers. If active currents do not significantly change the amplitude of presynaptic pulses, one can then predict that the distal end of an inhibitor branch would be depolarized to -8.4 mV while the presynaptic V electrode records a pulse depolarized from -70 to 0 mV. Because our D-R coupling data are enveloped by the D-R coupling curves with a space constant of 8 as lower limit, many of our preparations should have a space constant that is >8 . The 8.4-mV deviation can therefore be considered to be a high estimate and, therefore, this deviation lies in a similar range to that of the squid giant synapse, ~ 4.5 mV at 0 mV presynaptic depolarization (see Fig. 5 of Augustine et al. 1985b). This level of presynaptic space clamp of the crayfish inhibitor can closely approximate that which has been achieved in the squid giant synapse.

The absolute length of the space constant of inhibitor branches on a given muscle fiber can be estimated as follows. A typical central muscle fiber has a length of 500–600 μm . It is normally innervated by tertiary branches near its midpoint and the terminal branches rarely extend to the end of a muscle fiber. The distal end of a typical inhibitor terminal on a muscle fiber is therefore at most 250 μm from its proximal end. Allowing for an additional 50–100 μm for

the distance between the V electrode and the point where the proximal end of a tertiary axon contacts a muscle fiber, the presynaptic voltage clamp appears to be able to control 350 μm of an inhibitor branch “downstream” of the V electrode. With a space constant ≥ 8 times longer than its physical length, the space constant on the terminal branch should be ≥ 2.8 mm. This estimate is longer than that predicted from a previous study, ~ 1.3 mm (Wojtowicz and Atwood 1984). Although the space constant estimated by Wojtowicz and Atwood was based on a DC model and therefore should be considered to be an upper limit, the longer space constant estimated in this report could be attributed to the presence of potassium channel blockers. Because short and action-potential-like 2-ms presynaptic pulses could activate IPSPs with amplitudes similar to those activated by action potentials, one can assume that the extent of presynaptic filtering on 2- to 5-ms pulses is minimal (also see Sivaramakrishnan et al. 1991). In conclusion, presynaptic potentials controlled at the point of the secondary branch could presumably depolarize the terminal varicosities consistently and the local calcium influx was not large enough to generate uncontrolled spikes.

Experimental conditions needed to achieve optimal control of presynaptic potential

In the course of developing this preparation, we encountered many difficulties. With the use of the presence of suppression in $IPSP_{cor}$ as the main criterion, we found the following conditions to be essential for achieving optimal control: small animal, 15°C, and low $[Ca^{2+}]_o$. By the use of small animals, we restricted the length of presynaptic arborizations. Low $[Ca^{2+}]_o$ minimized the chance that calcium influx triggered uncontrolled spikes. Low temperature slowed down the calcium channel kinetics, which enabled the voltage-clamp circuit to control presynaptic potential better and avoid calcium spikes. In addition, low temperature increases membrane resistance, which should increase pre- and postsynaptic space constants.

Although it was possible to achieve suppression of $IPSP_{on}$ at room temperature and physiological levels of $[Ca^{2+}]_o$, we found that D-R coupling curves constructed from $IPSP$ peak amplitudes always gave rise to a plateau under these conditions. These conditions presumably still allow for reasonable control of presynaptic potential during the depolarizing pulses but the calcium influx associated with repolarization was probably no longer controlled. The uncontrolled “calcium spike” associated with repolarization would contribute to the plateauing phase of the D-R coupling curve.

Comparison with macropatch technique in the study of transmitter release

The technique reported here is not the only approach that can be used to study synaptic transmission in the absence of action potentials in the crayfish opener neuromuscular junction. Macropatch techniques have been used to investigate synaptic transmission and plasticity in the crayfish excitor (Dudel 1983, 1989a–d). However, this approach suffers two major limitations. First of all, the macropatch method is only adequate for depolarizing the presynaptic terminal

in an impulselike waveform. Because presynaptic potential is not monitored by this method, it is not able to compensate for the effects of potassium current, which may repolarize the terminal during a prolonged depolarizing pulse. The second main limitation relates to our intention to use our experimental method to study synaptic facilitation. The macropatch technique cannot avoid activating both excitator and inhibitor simultaneously and quantitative analysis of facilitation under such conditions creates uncertainties due to presynaptic inhibition (Dudel 1983; Dudel and Kuffler 1961b; unpublished observations). On the other hand, the macropatch technique has the advantage of monitoring transmitter release from a short segment of an axon and minimizing the spatial nonuniformity of the presynaptic branch under investigation. Ideally, one would like to combine both approaches, i.e., using two-electrode voltage clamp to control presynaptic potential and using macropatch recordings to monitor release from a short stretch of the inhibitor. Our attempts in this direction are at an embryonic stage. Given these technical considerations, the experimental conditions and criteria outlined in this report demonstrate that the presynaptic control method developed here can provide a reliable starting point for further explorations of synaptic plasticity.

This work was supported by Boston University fund 20617 and National Institute of Neurological Disorders and Stroke Grant NS-31707 to J.-W. Lin. A. Vyshedskiy is a graduate student at the Department of Biomedical Engineering, Boston University.

Address for reprint requests: J.-W. Lin, Dept. of Biology, Boston University, 5 Cummington St., Boston, MA 02215.

Received 21 May 1996; accepted in final form 19 September 1996.

REFERENCES

- ADELSBERGER, H., VON BECKERATH, N., PARZEFALL, F., AND DUDEL, J. A molecular scheme for the reaction between gamma-aminobutyric acid and the most abundant chloride channel on crayfish deep extensor abdominal muscle. *Pfluegers Arch.* 431: 680–689, 1996.
- ARAQUE, A., CLARAC, F., AND BUNO, W. P-type Ca^{2+} channels mediate excitatory and inhibitory synaptic transmitter release in crayfish muscle. *Proc. Natl. Acad. Sci. USA* 91: 4224–4228, 1994.
- ATWOOD, H. L. AND BITTNER, G. D. Matching of excitatory and inhibitory inputs to crustacean muscle fibers. *J. Neurophysiol.* 34: 157–170, 1970.
- ATWOOD, H. L., DIXON, D., AND WOJTCOWICZ, J. M. Rapid introduction of long-term synaptic changes at crustacean neuromuscular junction. *J. Neurobiol.* 20: 373–385, 1989.
- ATWOOD, H. L. AND WOJTCOWICZ, J. M. Short-term and long-term plasticity and physiological differentiation of crustacean motor synapses. *Int. Rev. Neurobiol.* 28: 275–362, 1986.
- AUGUSTINE, G. J., CHARLTON, M. P., AND SMITH, S. J. Calcium entry into voltage-clamped presynaptic terminals of squid. *J. Physiol. Lond.* 367: 143–162, 1985a.
- AUGUSTINE, G. J., CHARLTON, M. P., AND SMITH, S. J. Calcium entry and transmitter release at voltage-clamped nerve terminals of squid. *J. Physiol. Lond.* 367: 163–181, 1985b.
- BITTNER, G. D. Synaptic plasticity at the crayfish opener neuromuscular preparation. *J. Neurobiol.* 20: 386–406, 1989.
- BLIGHT, A. R. AND LLINAS, R. The non-impulsive stretch-receptor complex of the crab: a study of depolarization-release coupling at a tonic sensorimotor synapse. *Philos. Trans. R. Soc. Lond. B Biol. Sci.* 290: 219–276, 1981.
- BLUNDON, J. A., WRIGHT, S. N., BRODWICK, M. S., AND BITTNER, G. D. Presynaptic calcium-activated potassium channels and calcium channels at the crayfish neuromuscular junction. *J. Neurophysiol.* 73: 178–189, 1995.
- BORGES, S., GLEASON, E., TURELLI, M., AND WILSON, M. The kinetics of quantal transmitter release from retinal amacrine cells. *Proc. Natl. Acad. Sci. USA* 92: 6896–6900, 1995.
- BROSIUS, D. C., HACKETT, J. T., AND TUTTLE, J. B. Presynaptic calcium currents evoking quantal transmission from avian ciliary ganglion neurons. *Synapse* 5: 313–323, 1990.
- CHARLTON, M., SMITH, S. J., AND ZUCKER, R. S. Role of presynaptic calcium ions and channels in synaptic facilitation and depression at the squid giant synapse. *J. Physiol. Lond.* 323: 173–193, 1982.
- DELANEY, K. R., ZUCKER, R. S., AND TANK, D. W. Calcium in motor nerve terminals associated with posttetanic potentiation. *J. Neurosci.* 9: 3558–3567, 1989.
- DIETZEL, I. D., DRAPEAU, P., AND NICHOLLS, J. G. Voltage dependence of 5-hydroxytryptamine release at a synapse between identified leech neurons in culture. *J. Physiol. Lond.* 372: 191–205, 1986.
- DUDEL, J. Graded or all-or-nothing release of transmitter quanta by local depolarizations of nerve terminals on crayfish muscle? *Pfluegers Arch.* 398: 155–164, 1983.
- DUDEL, J. Calcium dependence of quantal release triggered by graded depolarization pulses to nerve terminals on crayfish and frog muscle. *Pfluegers Arch.* 415: 289–298, 1989a.
- DUDEL, J. Shifts in the voltage dependence of synaptic release due to changes in the extracellular calcium concentration at nerve terminals on muscle of crayfish and frogs. *Pfluegers Arch.* 415: 299–303, 1989b.
- DUDEL, J. Calcium and depolarization dependence of twin-pulse facilitation of synaptic release at nerve terminal of crayfish and frog muscle. *Pfluegers Arch.* 415: 304–309, 1989c.
- DUDEL, J. Twin pulse facilitation in dependence on pulse duration and calcium concentration at motor nerve terminals of crayfish and frog. *Pfluegers Arch.* 415: 310–315, 1989d.
- DUDEL, J. AND HATT, H. Four types of GABA receptors in crayfish leg muscles characterized by desensitization and specific antagonist. *Pfluegers Arch.* 364: 217–222, 1976.
- DUDEL, J. AND KUFFLER, S. W. Mechanisms of facilitation at the crayfish neuromuscular junction. *J. Physiol. Lond.* 155: 530–542, 1961a.
- DUDEL, J. AND KUFFLER, S. W. Presynaptic inhibition at the crayfish neuromuscular junction. *J. Physiol. Lond.* 155: 543–562, 1961b.
- DUNLAP, K., LUEBKE, J. L., AND TURNER, T. J. Exocytotic Ca^{2+} channels in mammalian central neurons. *Trends Neurosci.* 18: 89–98, 1995.
- FINGER, W. AND STETTMEIER, H. Analysis of miniature spontaneous inhibitory postsynaptic currents (sIPSCs) from current noise in crayfish opener muscle. *Pfluegers Arch.* 392: 157–162, 1981.
- FLOREY, E. AND CAHILL, M. A. The innervation pattern of crustacean skeleton muscle. *Cell Tissue Res.* 224: 527–541, 1982.
- FUCHS, P. A. AND GETTING, P. A. Ionic basis of presynaptic inhibitory potentials at crayfish claw opener. *J. Neurophysiol.* 43: 1547–1557, 1980.
- GOLAN, H. AND GROSSMAN, Y. Block of GABA-transaminase modifies GABAergic transmission at the crayfish synapses. *J. Neurophysiol.* 71: 48–58, 1994.
- GOVIND, C. K., ATWOOD, H. L., AND PEARCE, J. Inhibitory axoaxonal and neuromuscular synapses in the crayfish opener muscle: membrane definition and ultrastructure. *J. Comp. Neurol.* 351: 476–488, 1995.
- GROSSMAN, Y., COLTON, J. S., AND GILMAN, S. C. Interaction of Ca-channel blockers and high pressure at the crustacean neuromuscular junction. *Neurosci. Lett.* 125: 53–56, 1991.
- HAYASHI, J. H., MOORE, J. W., AND STUART, A. E. Adaptation in the input-output relation of the synapse made by the barnacle's photoreceptor. *J. Physiol. Lond.* 368: 179–195, 1985.
- HAYDON, P. G. Chemical synapses form between isolated neuronal somata in the absence of neurite extension. *J. Neurosci.* 8: 329–341, 1988.
- HONG, S. J. AND LLENICKA, G. A. Activity-dependent reduction in voltage-dependent calcium current in a crayfish motoneuron. *J. Neurosci.* 15: 3539–3547, 1995.
- KAILA, K. AND VOIPIO, J. Postsynaptic fall in intracellular pH induced by GABA-activated bicarbonate conductance. *Nature Lond.* 330: 163–165, 1987.
- KATZ, B. AND MILEDI, R. Tetrodotoxin-resistant electric activity in presynaptic terminals. *J. Physiol. Lond.* 203: 459–487, 1969.
- LANDO, L. AND ZUCKER, R. S. Ca^{2+} cooperativity in neurosecretion measured using photolabile Ca^{2+} chelators. *J. Neurophysiol.* 72: 825–830, 1994.
- LIN, J. AND LLINAS, R. Depolarization-activated potentiation of the T-fiber synapse in the blue crab. *J. Gen. Physiol.* 101: 45–65, 1993.
- LLINÁS, R., STEINBERG, I. Z., AND WALTON, K. Presynaptic calcium current in squid giant synapse. *Biophys. J.* 33: 289–322, 1981a.
- LLINÁS, R., STEINBERG, I. Z., AND WALTON, K. Relationship between pre-

- synaptic calcium current and postsynaptic potential in squid giant synapse. *Biophys. J.* 33: 323–352, 1981b.
- LORENZON, N. M. AND FOEHRING, R. C. Characterization of pharmacologically identified voltage-gated calcium channel currents in acutely isolated rat neocortical neurons. I. Adult neurons. *J. Neurophysiol.* 73: 1430–1442, 1995.
- MARTIN, A. R. A further study of the statistical composition of the endplate potential. *J. Physiol. Lond.* 130: 114–122, 1955.
- MCLACHLAN, E. M. AND MARTIN, A. R. Non-linear summation of end-plate potentials in the frog and mouse. *J. Physiol. Lond.* 311: 307–324, 1981.
- MINTZ, I. M., SABATINI, B. L., AND REGEHR, W. G. Calcium control of transmitter release at a cerebellar synapse. *Neuron* 15: 675–688, 1995.
- SCHWEIZER, F., BETZ, H., AND AUGUSTINE, G. From vesicle docking to exocytosis: intermediate reactions of exocytosis. *Neuron* 14: 686–696, 1995.
- SIMON, S. M. AND LLINAS, R. R. Compartmentalization of the submembrane calcium activity during calcium influx and its significance in transmitter release. *Biophys. J.* 48: 485–498, 1985.
- SIVARAMAKRISHNAN, S., BITTNER, G. D., AND BRODWICK, M. S. Calcium-activated potassium conductance in presynaptic terminals at the crayfish neuromuscular junction. *J. Gen. Physiol.* 98: 1161–1179, 1991.
- SMITH, S. J., AUGUSTINE, G. J., AND CHARLTON, M. P. Transmission at voltage-clamped giant synapse of the squid: evidence for cooperativity of presynaptic calcium action. *Proc. Natl. Acad. Sci. USA* 82: 622–625, 1985.
- SUDHOF, T. C. The synaptic vesicle cycle: a cascade of protein-protein interactions. *Nature Lond.* 375: 645–653, 1995.
- SWANDULLA, D., HANS, M., ZIPSER, K., AND AUGUSTINE, G. J. Role of residual calcium in synaptic depression and potentiation: fast and slow calcium signaling in nerve terminals. *Neuron* 7: 915–926, 1991.
- TAKEUCHI, A. AND TAKEUCHI, N. Electrical changes in pre- and post-synaptic axons of the giant synapse of *Loligo*. *J. Gen. Physiol.* 45: 1181–1193, 1962.
- THOMPSON, S. M., MASUKAWA, L. M., AND PRINCE, D. A. Temperature dependence of intrinsic membrane properties and synaptic potentials in hippocampal CA1 neurons in vitro. *J. Neurosci.* 5: 817–824, 1985.
- WOJTOWICZ, J. M. AND ATWOOD, H. L. Presynaptic membrane potential and transmitter release at the crayfish neuromuscular junction. *J. Neurophysiol.* 52: 99–113, 1984.
- WOJTOWICZ, J. M. AND ATWOOD, H. L. Long-term facilitation alters transmitter releasing properties at the crayfish neuromuscular junction. *J. Neurophysiol.* 55: 484–498, 1986.
- WRIGHT, S. N., BRODWICK, M. S., AND BITTNER, G. D. Presynaptic calcium current and neurotransmitter release at voltage clamped terminals of crayfish neuromuscular junction. *Soc. Neurosci. Abstr.* 20: 901, 1994.
- WU, L.-W. AND SAGGAU, P. Pharmacological identification of two types of presynaptic voltage-dependent calcium channels at CA3-CA1 synapses of the hippocampus. *J. Neurosci.* 14: 5613–5622, 1994.
- YAMADA, M. W. AND ZUCKER, R. S. Time course of transmitter release calculated from simulations of a calcium diffusion model. *Biophys. J.* 61: 671–682, 1992.